10308 *Biochemistry* **2010,** *49,* 10308–10318
DOI: 10.1021/bi1011755

BIOCHEMISTRY
including biophysical chemistry & molecular biology
Article

Electrophysiology of Respiratory Chain Complexes and the ADP−ATP Exchanger in Native Mitochondrial Membranes

Natalie Watzke,[‡] Kerstin Diekert,[‡] and Petr Obrdlik*[,‡]

IonGate Biosciences GmbH, Industriepark Hoechst, D528, 65926 Frankfurt am Main, Germany.
[‡]Present address: Scientific Devices Heidelberg GmbH, Schlosskirschenweg 24-26, 69124 Heidelberg, Germany.

Received July 24, 2010; Revised Manuscript Received October 12, 2010

ABSTRACT: Transport of protons and solutes across mitochondrial membranes is essential for many physiological processes. However, neither the proton-pumping respiratory chain complexes nor the mitochondrial secondary active solute transport proteins have been characterized electrophysiologically in their native environment. In this study, solid-supported membrane (SSM) technology was applied for electrical measurements of respiratory chain complexes CI, CII, CIII, and CIV, the F_OF_1-ATPase/synthase (CV), and the adenine nucleotide translocase (ANT) in inner membranes of pig heart mitochondria. Specific substrates and inhibitors were used to validate the different assays, and the corresponding $K_{0.5}$ and IC_{50} values were in good agreement with previously published results obtained with other methods. In combined measurements of CI−CV, it was possible to detect oxidative phosphorylation (OXPHOS), to measure differential effects of the uncoupler carbonyl cyanide *m*-chlorophenylhydrazone (CCCP) on the respective protein activities, and to determine the corresponding IC_{50} values. Moreover, the measurements revealed a tight functional coupling of CI and CIII. Coenzyme Q (CoQ) analogues decylubiquinone (DBQ) and idebenone (Ide) stimulated the CII- and CIII-specific electrical currents but had inverse effects on CI−CIII activity. In summary, the results describe the electrophysiological and pharmacological properties of respiratory chain complexes, OXPHOS, and ANT in native mitochondrial membranes and demonstrate that SSM-based electrophysiology provides new insights into a complex molecular mechanism of the respiratory chain and the associated transport proteins. Besides, the SSM-based approach is suited for highly sensitive and specific testing of diverse respiratory chain modulators such as inhibitors, CoQ analogues, and uncoupling agents.

Mitochondria play a central role in the cellular energy metabolism by providing the cell with ATP, the molecular unit of currency of intracellular energy transfer. The underlying reaction is the oxidative phosphorylation (OXPHOS),[1] in which the oxidation of reduced substrate NADH or $FADH_2$ finally leads to the phosphorylation of ADP by inorganic phosphate (*1*). The outer and inner membranes surround each mitochondrion, defining the intermembrane space between them. The proteins participating in OXPHOS are respiratory chain complexes CI, CII, CIII, and CIV and the F_OF_1-ATPase (CV), all localized in the inner membrane. CI, CIII, and CIV are pumps moving protons across the inner membrane to the intermembrane space. The resulting electrochemical proton gradient serves as the driving force for the ATP synthesis catalyzed by the F_OF_1-ATPase. Newly synthesized ATP can subsequently leave the mitochondria through the adenine nucleotide translocase ANT [ADP−ATP carrier (AAC) and adenine nucleotide carrier (ANC)] in exchange for ADP (*2*, *3*).

Activities of respiratory chain proteins are coordinated, and changes in one complex can influence the activities of the others (*4*, *5*). Therefore, studies of their activities in native surroundings, i.e., mitochondrial membranes, can provide new insight into the regulation of OXPHOS and respiration. The translocation of protons through the OXPHOS complexes as well as the ANT transport activity generates membrane potential and is therefore amenable to electrophysiological analysis. However, electrophysiological studies of inner mitochondrial membranes with standard techniques are very limited because of the poor accessibility of the membranes. For classical patch−clamp experiments, either mitoplasts or mitochondrial membranes incorporated into giant liposomes were used (*6*−*9*). Alternatively, some patch−clamp studies used purified mitochondrial transport proteins reconstituted in giant liposomes (*10*, *11*). Such studies are technically challenging and, until now, applicable only to channel proteins or the channel activity of secondary active solute transporters and/or carriers. On the other hand, two pilot studies had demonstrated that the solid-supported membrane (SSM) technology is suited for electrical measurements of mitochondrial transport proteins reconstituted in proteoliposomes (*12*, *13*). Despite these studies, to date there is no report of the electrical analysis of respiratory chain complexes and related transport proteins in their native environment.

The core of the technique is the SSM, consisting of a gold electrode coated with an alkane thiol and a phospholipid layer on top of it (*14*, *15*). Biological membranes containing the transport protein(s) of interest are then adsorbed onto this SSM sensor,

*To whom correspondence should be addressed: Schlosskirschenweg 24-26, 69124 Heidelberg, Germany. E-mail: petrobrdlik@web.de. Telephone: +49 (0)6221-7183139. Fax: +49-(0)6221-7183179.

[1]Abbreviations: SSM, solid-supported membrane; NADH, nicotinamide adenine dinucleotide; DTT, dithiothreitol; NMG, *N*-methylglucosamine; K-gluconate, potassium gluconate; OXPHOS, oxidative phosphorylation.

 Published on Web 10/19/2010

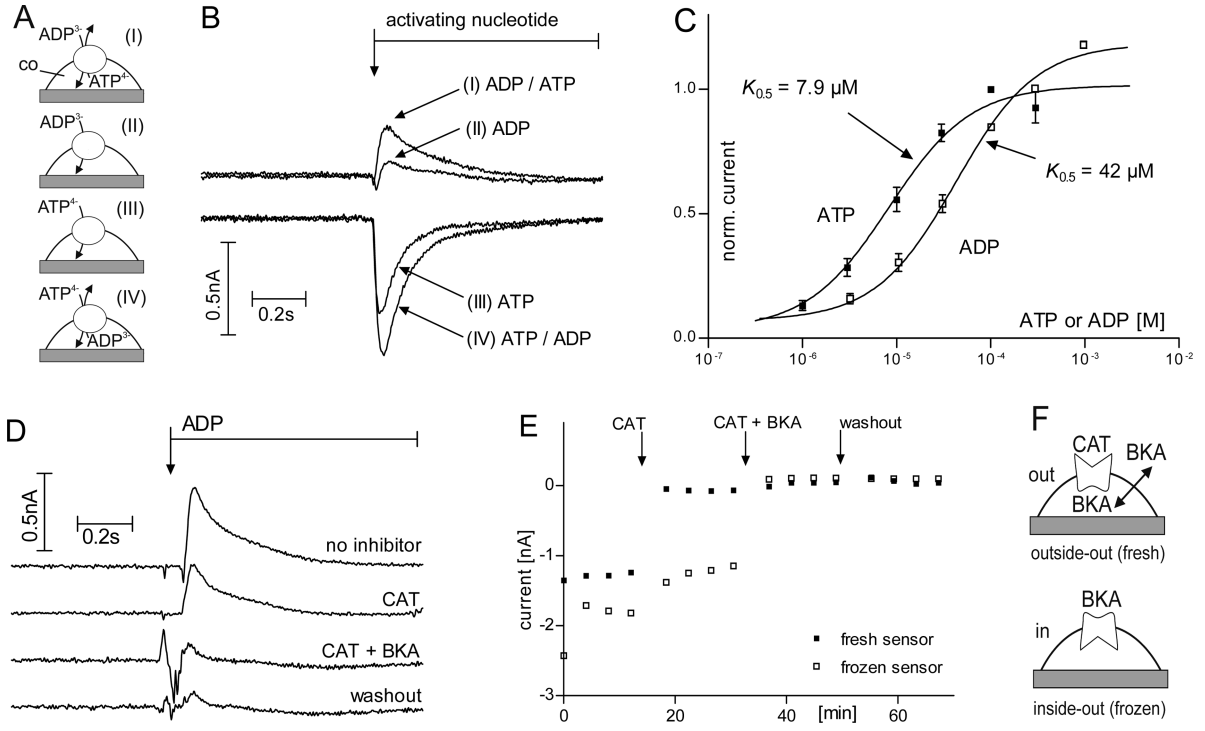

FIGURE 1: Electrical measurements and pharmacology of the ANT activity and sidedness of the inner membranes on sensors. (A) Pictogram showing the arrangement of the membranes on the sensors, and the applied assay conditions (I−IV) for ANT. The gray bottom bar indicates the SSM-covered sensor electrode, and the curved line above symbolizes the mitochondrial membrane with the embedded ANT protein (white circles). A fluid-filled compartment (co) is formed between the SSM and the mitochondrial membrane. The arrows indicate the direction of transport of the nucleotide into or out of the compartment under different assay conditions. (B) ANT-dependent currents under conditions I−IV as described for panel A. The nucleotides were at a concentration of 300 μM. The top bar indicates the flow of the activating solution containing either ADP (I and II) or ATP (III and IV). (C) Dependence of the currents on ATP (■) and ADP (□) as measured in the presence of outward-directed ADP and ATP counter gradients, respectively. Currents were normalized relative to the currents at 300 μM nucleotide. Results are means ± the standard error of the mean for three to five experiments at each concentration. (D) Inhibition of ADP-induced currents with CAT and BKA (5 μM). The top bar indicates the flow of the activating solution. "Frozen" sensors were used for panels A−D. (E) Effect of sensor freezing on the CAT and BKA inhibition. ANT was activated via ATP jumps (300 μM) . The ANT activity (peak current) was repeatedly recorded on the same sensors over an extended time period in the absence of inhibitors, in the presence of CAT, in the presence of CAT and BKA, and in absence of inhibitors. Arrows indicate the corresponding buffer changes. (F) Preferential sidedness of the membranes on fresh and frozen sensors as determined by the side-specific inhibitors CAT and BKA. CAT is membrane impermeable and binds to the intermembrane face (outside) of ANT. BKA is membrane permeable and binds to the matrix face (inside) of ANT.

thereby forming fluid-filled compartments between the membranes and the SSM (Figure 1A). The protein-specific charge movements into or out of these compartments are induced by substrate concentration jumps and measured as transient electrical currents. The transient nature of the currents is due to the biosensor assembly in which the gold electrode and the fluid of the compartment represent capacitor plates. Accordingly, the protein-dependent currents correspond to the charging of these capacitor plates. The kinetics of the currents depends on the activity and mechanistic properties of the tested transport protein, whereas the polarity of the translocated charge(s) and the direction of their transport determine the sign of the detected currents (*16*, *17*). Usually, peak current amplitudes are used for the analysis of transport activity.

In this work, we developed SSM-based protocols for measuring transporters and pumps in native inner mitochondrial membranes. These protocols were applied to investigate the functional mechanism of respiratory chain complexes CI, CII, CIII, and CIV, F_OF_1-ATPase (CV), and ANT. Furthermore, ATP synthesis (OXPHOS) was analyzed by measuring electrical currents induced via combined activation of complexes CI, CIII, CIV, and CV. This assay was also used to study the effect of uncouplers on the OXPHOS machinery.

MATERIALS AND METHODS

Isolation of Mitochondria. Mitochondria were isolated by a modified procedure of Blair et al. (*18*). Fresh porcine heart was washed with an ice-cold 9% NaCl solution and stored on ice. Veins and fat were removed before the muscle tissue was diced. Approximately 70 g of heart muscle tissue was combined with 150 mL of cold buffer I [250 mM sucrose, 10 mM Tris (pH 7.4), and "Complete" protease inhibitor mix (Roche)], added to a pre-cooled blender (Waring), and homogenized at 20000 rpm for 1 min. The homogenate was filtered through a polycarbonate net. Cold buffer I was added to the filtered suspension to give a final volume of 250 mL and then the mixture homogenized using a Teflon−glass homogenizer (250 rpm, 25 strokes). The homogenate was centrifuged at 1500*g* for 10 min at 4 °C. The supernatant was filtered and centrifuged at 25000*g* for 15 min at 4 °C. The remaining pellet was composed of three brown layers. The top light-brown layer consisting of mitochondria was resuspended in buffer II [250 mM sucrose, 20 mM Tris (pH 7.4), 0.2 mM EDTA, and 1 mM succinate] and homogenized with the Teflon−glass homogenizer (250 rpm, 10 strokes), and the resulting suspension was centrifuged at 25000*g* for 15 min at 4 °C. The last two steps were repeated to remove microsomes, hemoglobin, and myoglobin.

The resulting pellet was resuspended in buffer II, aliquoted in 2 mL samples, and frozen in liquid nitrogen.

Preparation of Inner Mitochondrial Membranes. The outer and inner mitochondrial membranes were separated by a modified "swell−shrink−sonicate" procedure (*19*). Two milliliters of the purified mitochondria was thawed and centrifuged at 4 °C (25000*g* for 15 min). The pellet was resuspended in 6 mL of 10 mM Tris (pH 7.4) and incubated on ice while being stirred for 15 min. Then, 6 mL of buffer III [32% sucrose (w/v), 30% glycerol (v/v), 10 mM $MgCl_2$, and 10 mM Tris (pH 7.4)] was added, and the suspension was incubated for an additional 15 min while being stirred. The suspension was sonicated (five bursts with a 15 s duration with 1 min intervals, on ice) using a Dr. Hielscher UP 50 H instrument equipped with an MS1 tip at 70% amplitude. The suspension was centrifuged at 12000*g* for 10 min at 4 °C. The supernatant [inner membranes (IM) and matrix] was further purified on a discontinuous sucrose gradient. For the loading, the pellet was resuspended in 8 mL of mannitol buffer [250 mM mannitol, 0.5 mM EGTA, 0.1% (w/v) BSA, and 10 mM Tris (pH 7.4)]. The sucrose gradients consisted of 2 mL of 25.3, 37.7, or 51.3% (w/v) sucrose in 10 mM Tris (pH 7.4). The gradients were spun at 210000*g* for 3 h at 4 °C. The inner membranes were collected in the 51.3% layer. The fractions were diluted 3-fold with mannitol buffer and centrifuged at 12000*g* for 15 min at 4 °C. The resulting IM-enriched pellet was resuspended in mannitol buffer, and the protein content was determined by a BCA assay (Pierce). Aliquots corresponding to ~100 μg of total protein were stored at −80 °C.

SSM Sensor Preparation. The biosensors were prepared with gold electrode sensors from IonGate Biosciences as described by the manufacturer. Briefly, the sensors were first covered with an alkane thiol followed by a phosholipid diphytanoylphosphatidylcholine (*15*). Then, the sensor wells were filled immediately with 50 μL of equilibrating buffer [140 mM NaCl, 2 mM $MgCl_2$, and 30 mM Hepes (pH 7.2)] and incubated at 4 °C for 15 min. An aliquot of purified inner mitochondrial membranes (IM) was quickly thawed and diluted to a final protein concentration of 0.5−1 μg/μL in equilibrating buffer. Optionally, the buffer contained 5 μM BKA (bongkrekic acid) to irreversibly block ANT. Diluted IM were resuspended and homogenized by pipetting up and down 30 times, and 5 μL of the suspension was applied to the sensor surface. The sensors were centrifuged at 2500*g* for 45 min at 6 °C. The biosensors were either stored at 4 °C for 2−4 days or frozen at −80 °C for several months. In the latter case, the biosensors were thawed immediately prior to the experiment. As described in Results, the freezing of the sensors altered the ratio of inside-out (matrix-side-out) versus outside-out (intermembrane-side-out) IM on the sensors. Accordingly, it is noted in the text where "fresh" (4 °C) or "frozen" (−80 °C) sensors were used.

Electrical Measurements and Data Analysis. For electrical measurements, the IM-loaded biosensors were integrated into the fluidic system of the *SURFE²R WORKSTATION* setup (Surface Electrogenic Event Reader, IonGate Biosciences), and the transport proteins were activated via rapid exchange among preincubating (C), nonactivating (N), and activating (A) solutions at a flow rate of 200−300 μL/s (*16*, *17*). The application of solution A induced transient rapidly decaying currents. After the current decayed, rinsing the sensor with the C or N solution returned the system to the preactivation state. By repeating such solution exchange protocols, we could analyze different solutions and experimental conditions on the same sensor for extended time periods (4−8 h). If required, reference measurements were performed to monitor possible loss (run down) of the protein activity during the experimental period. The individual assay conditions were as follows. (i) ANT-specific currents were induced by exchange of solution N [150 mM K-gluconate, 30 mM Hepes (pH 7.2/NMG)] for solution A (solution N supplemented with 300 μM ADP or ATP). For measurements in the presence of outward-directed ATP or ADP counter gradients, sensors were equilibrated with solution C (solution N supplemented with 300 μM ADP or ATP) prior to the application of solution N. (ii) F_OF_1-ATPase in reverse mode was measured on BKA (5 μM)-treated sensors by exchanging solution N [140 mM K-gluconate, 10 mM $MgCl_2$, 30 mM Hepes (pH 7.2/NMG)] for solution A (solution N supplied with 300 μM ATP). (iii) Proton pumping respiratory chain complexes CI and CIII were activated by NADH concentration jumps using solution N [140 mM K-gluconate, 2 or 10 mM $MgCl_2$, 0 or 12.5 mM KP_i, 30 mM Hepes (pH 7.2/NMG)] and solution A (solution N with 100 μM NADH). (iv) CIV was activated by reduced cytochrome *c* with solution N [140 mM NaCl, 2 mM $MgCl_2$, 60 μM ascorbate, 30 mM Hepes (pH 7.2/NMG)] and solution A (3 μM reduced cytochrome *c* in solution N). (v) The CII−CIII reaction was trigged by 3 μM oxidized cytochrome *c* added to solution N [150 mM K-gluconate, 10 mM $MgCl_2$, 12 mM KP_i, 30 mM Hepes (pH 7.2/NMG)]. (vi) ATP synthesis (OXPHOS) was activated by first equilibrating the sensors in solution C [150 mM K-gluconate, 10 mM $MgCl_2$, 12 mM KP_i, 30 mM Hepes (pH 7.2/NMG)] and then exchanging solution C for solution N (solution C supplied with 100 μM NADH) and solution A (solution C supplemented with 100 μM NADH and 300 μM ADP). Inhibitors were prepared as DMSO stock solutions (rotenone and oligomycin) or ethanol stock solutions (antimycin) and added in equimolar amounts to all solutions. The final concentration of DMSO or ethanol in solutions never exceeded 0.1%. KCN and NaN_3 were added directly to the solutions. The corresponding amounts of DMSO or ethanol were added to the solutions also for the control experiments without inhibitors. To prevent precipitation, idebenone (Ide) and DBQ were applied in the presence of 350 mg/L BSA and 0.01% DMSO to the solutions. Alternatively, DBQ was applied in the absence of BSA, and the solutions were stirred extensively. For the quantification of the effects of Ide and DBQ on CII−CIII or CI−CIII activities, the currents were repeatedly recorded over a time period of ~15 min and the last five recordings were then used for the analysis.

Experiments for kinetic studies were performed in at least triplicate, with the full range of substrate or inhibitor concentrations being tested on each single sensor, and such a titration curve was repeated on at least three different sensors. To calculate the apparent $K_{0.5}$ and IC_{50} values, we fit the data to a sigmoidal dose−response function (Hill equation). Unless otherwise stated, the Hill coefficient was set to 1. All current trace diagrams show serial measurements recorded on the same sensor and are representative of at least three independent experiments. Histograms represent at least three independent experiments.

RESULTS

ANT and the Orientation of Membranes on Biosensors. In mitochondria, the adenine nucleotide translocase ANT is responsible for the electrogenic exchange of ATP^{4-} versus ADP^{3-} ("heteroexchange mode"). Besides, earlier SSM-based studies using ANT-containing proteoliposomes showed that the carrier

Table 1: Apparent Affinities and Inhibition Values Determined with the SSM-Based Assays

protein	substrate or inhibitor	$K_{0.5}$ or IC_{50} (Hill coefficient)[a]
ANT	ADP[b]	42 ± 4 μM
	ATP[b]	7.9 ± 1.2 μM
	ATP[c]	8.3 ± 1.0 μM
F_OF_1-ATPase	ATP	45 ± 5 μM
	azide	13 ± 1 μM
CI−CIII	NADH	17 ± 2 μM
	rotenone	782 ± 30 pM (1.7 ± 0.1)
	antimycin A	27 ± 3 nM (1.8 ± 0.3)
	CCCP	305 ± 60 nM
CII−CIII	succinate	2.5 ± 0.7 μM
	antimycin A	9.6 ± 1.7 nM (1.7 ± 0.4)
F_OF_1-ATP synthase	CCCP	3.5 ± 0.8 nM

[a]Absolute values of the Hill coefficient. If not otherwise stated, the Hill values were fixed to 1. [b]Measured in an exchange mode, with an ATP or ADP (300 μM) counter gradient. [c]Measured in a "one-direction mode" in the absence of an ADP counter gradient.

could also translocate only ATP^{4-} or only ADP^{3-} in the absence of the other nucleotide (*13*). We adapted the described SSM-based protocols to test the ANT activity on SSM sensors coated with native inner mitochondrial membranes (IM). For the hetero-exchange mode measurements, the sensors were equilibrated with either ATP or ADP (300 μM). Subsequently, a nucleotide-free nonactivating solution was applied, thereby generating an outward-directed ATP or ADP counter gradient (Figure 1A). The nonactivating solution was then exchanged for an activating solution containing either ADP or ATP (300 μM), correspondingly. For measurement of the transport of only one type of nucleotide, the sensor was equilibrated with nucleotide-free nonactivating solution and ANT was activated with either ADP or ATP concentration jumps. Consistent with previous SSM-based studies on proteoliposomes, ADP induced transient currents of opposite sign in contrast to ATP-induced currents [Figure 1B (*13*)]. Both ADP- and ATP-induced peak currents were significantly increased in the presence of ATP and ADP counter gradients, respectively (Figure 1B). The ATP dependence and the ADP dependence of the currents were determined by measuring the peak amplitudes at different ADP and ATP concentrations in the activating solution (Figure 1C and Table 1). In the presence of the ATP or ADP counter gradients, the $K_{0.5}^{ADP}$ of 42 μM was ~5 times higher than the $K_{0.5}^{ATP}$ of 7.9 μM. The same $K_{0.5}^{ATP}$ was obtained in the absence of the ADP counter gradient. The specificity of the currents was tested with ANT inhibitors carboxyatractyloside (CAT) and bongkrekic acid (BKA) (Figure 1D,E). The ADP-induced signal was partially inhibited by 5 μM CAT and fully inhibited by 5 μM BKA. While the inhibition by CAT was partially reversible (data not shown), BKA inhibition was irreversible within the time frame of the measurement.

Both freshly prepared biosensors and frozen biosensors stored at −80 °C after the adsorption of inner mitochondrial membranes can be used for the SSM measurements (Materials and Methods). On fresh sensors, CAT inhibited the ATP-induced currents by 80−100%, while the currents on frozen sensors were inhibited by 35−50% (Figure 1E). In contrast, BKA completely blocked the ATP-induced signal on the fresh and frozen sensors. CAT is membrane impermeable and binds specifically to the intermembrane face of the ANT protein. Consequently, CAT can access only intermembrane-side-out (outside-out) ANT proteins on the sensors (Figure 1F). In comparison to CAT, BKA is fully membrane permeable and binds to ANT on the matrix side and can therefore inhibit ANT in intermembrane-side-out as well as matrix-side-out membranes. The results of CAT inhibition experiments indicate that the freezing of biosensors increases the portion of matrix-side-out (inside-out) membranes on the sensors (Figure 1F). Therefore, in the following experiments, fresh sensors were used if the intermembrane-side-out orientation was preferred, whereas frozen sensors were used if either both orientations or the matrix-side-out orientation was required.

F_OF_1-ATPase and ATP Hydrolysis. The F_OF_1-ATPase (complex V, CV) can either synthesize ATP from ADP and P_i ("forward" mode) or function as an ATPase hydrolyzing ATP to ADP and P_i ("reverse" mode) (*20*, *21*). In the following experiments, the ATPase (reverse) mode was studied.

Two major aspects were taken into account when the F_OF_1-ATPase assay was designed. First, because the ATP binding site is localized at the matrix face of the protein, the F_OF_1-ATPase can be activated via ATP concentration jumps only if the matrix side of the membranes faces the bath solution (Figure 2A). Therefore, frozen sensors with their increased content of matrix-side-out membranes were used (Figure 1F and Materials and Methods). Second, ATP concentration jumps not only will activate F_OF_1-ATPase but can also activate ANT (Figure 1B). To discriminate between these two ATP-dependent protein activities, we exploited the differential effect of Mg^{2+} on both transport systems (*13*, *21*). ATP concentration jumps induced positive transient currents in the presence of 10 mM $MgCl_2$ (Figure 2B), consistent with the SSM-based principles and with the movement of positive charges (protons) toward the sensor electrode. Removing Mg^{2+} from the buffers diminished the positive ATP-induced currents, and only ANT-specific negative currents were recorded (Figure 2B, top trace). Application of the ANT inhibitor BKA (5 μM) abolished the negative ANT-specific signal under Mg^{2+}-free conditions, while the positive current was still detected in the presence of Mg^{2+} (Figure 2B, bottom trace). Hence, the application of BKA and Mg^{2+}-containing solutions allowed F_OF_1-selective measurements. On BKA-treated sensors, ATP-induced currents were substrate-dependent with a calculated $K_{0.5}^{ATP}$ of 45 ± 5 μM and were fully inhibited by 1 mM azide (Figure 2C and Table 1). The calculated IC_{50}^{azide} was 13 ± 1 μM. For both $K_{0.5}^{ATP}$ and IC_{50}^{azide}, the absolute value of the Hill coefficient was ~1. The ATP-induced currents were fully inhibited by the F_OF_1-ATPase-specific inhibitor oligomycin [2 μM (Figure 2D)]. The effect of another F_OF_1-ATPase inhibitor *N*,*N*′-dicyclohexylcarbodiimide (DCCD) depended on the concentration and incubation time [Figure 2E (*22*)]. At 1 μM DCCD, the inhibition was slow and incomplete after incubation for ~10 min, whereas DCCD rapidly and fully inhibited the F_OF_1-ATPase-specific current at a concentration of 10 μM.

Coupled Measurements of Respiratory Chain Proton Pumps. The mitochondrial respiratory chain starts with complex CI (NADH dehydrogenase), catalyzing the oxidation of NADH, pumping protons across the membrane from the matrix into the intermembrane space, and in parallel reducing coenzyme Q (CoQ) (*23*). In subsequent reactions, the electrons of reduced CoQ are transferred to CIII (cytochrome bc_1 complex) and finally via cytochrome *c* (cyt *c*) to CIV (cytochrome *c* oxidase). Like in CI, the transfer of electrons in CIII and CIV is coupled to proton pumping from the matrix to the intermembrane space.

The CI protein was activated by NADH concentration jumps. Because the NADH binding site of CI is localized at the matrix

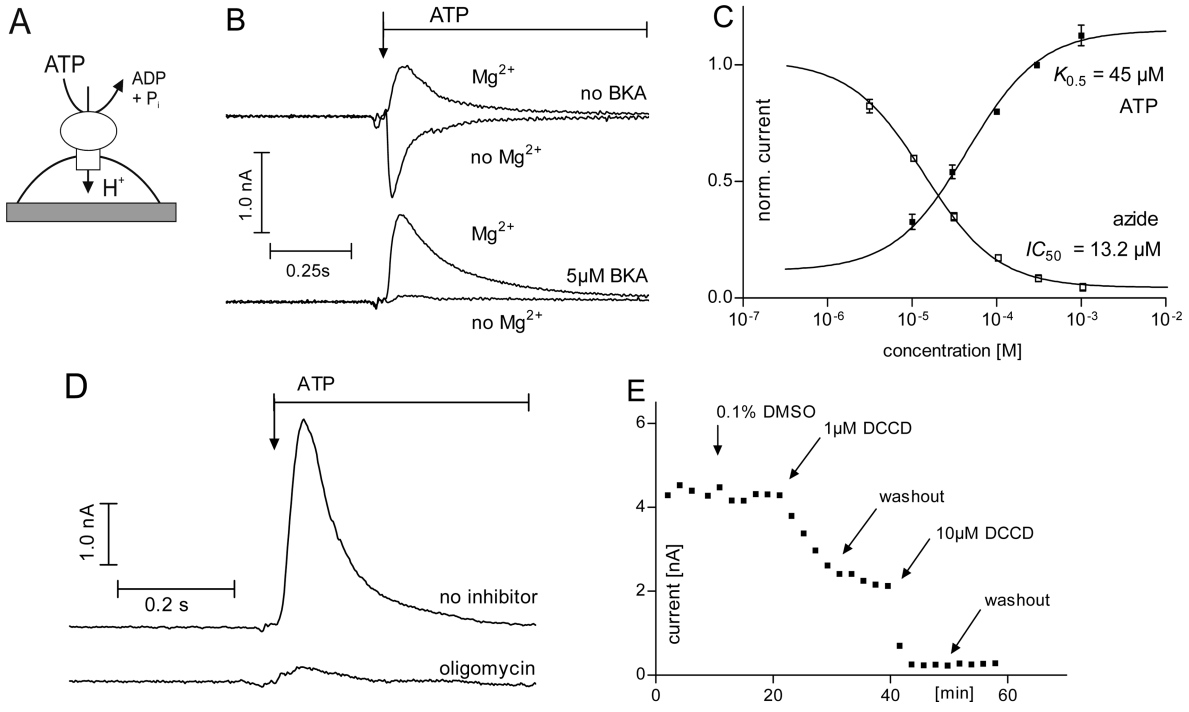

FIGURE 2: F_OF_1-ATPase activity in reverse mode. (A) Pictogram showing the ATP-induced transport of protons via F_OF_1-ATPase on SSM sensors. (B) Dependence of the ATP (300 μM)-induced currents on magnesium and ANT inhibitor BKA. The positive F_OF_1-dependent and negative ANT-dependent currents were measured in the presence and absence of Mg^{2+} (10 mM $MgCl_2$), respectively. On BKA (5 μM)-treated sensors, only F_OF_1-ATPase-dependent currents were detected. (C) Dependence of the ATP-induced currents on ATP (■) and the F_OF_1-ATPase inhibitor azide (□, NaN_3). In the case of ATP dependence, the currents were normalized relative to the currents at 300 μM ATP. For azide dependence, the currents were induced with 300 μM ATP in the presence of increasing NaN_3 concentrations and the currents were normalized relative to the current without the inhibitor. Results are means ± the standard error of the mean for three to four experiments at each concentration. (D) Inhibition of the ATP (300 μM)-induced currents with oligomycin (2 μM), as measured on BKA-treated sensors. (E) Inhibition of the ATP (300 μM)-induced currents with DCCD. The F_OF_1 activity was recorded over an extended period of time in the absence of additives, at 0.1% DMSO, 1 μM DCCD, 0.1% DMSO (washout), 10 μM DCCD, and final washout. Arrows indicate the corresponding buffer changes. For panels B−E, measurements were performed in the presence of 10 mM $MgCl_2$ on BKA (5 μM)-treated, matrix-side-out enriched sensors (inside-out, Figure 1). The top bars indicate the flow of the ATP-containing solution.

side of the protein, frozen sensors enriched in matrix-side-out oriented membranes were used (see above). The application of NADH (100 μM) induced positive electric currents, which was consistent with the flow of positive charges (protons) from the bath solution to the sensor electrode (Figure 3A,B). The CI-specific inhibitor rotenone (10 nM) fully blocked the NADH-induced current (Figure 3B). A simple washout procedure did not restore the observed current, but the addition of the CoQ analogue decylubiquinone (DBQ, 3 μM) to the washout solutions led to the recovery of the NADH-induced activity (Figure 3B). Apart from rotenone, also the CIII-specific inhibitor antimycin [300 nM (Figure 3C)] fully blocked the NADH-induced currents. As in the case of rotenone, the NADH-induced currents were re-established upon addition of 3 μM DBQ. In contrast, the blockage of the NADH-induced current with the CIV inhibitor KCN (1 mM) was fully reversible in the absence of DBQ (Figure 3D). The CIV inhibitor sodium azide (NaN_3, 1 mM) did not inhibit the NADH-induced currents (Figure 1 of the Supporting Information).

NADH-induced signals were further studied in terms of different CoQ analogues, NADH dependence, and inhibition kinetics. Two different CoQ analogues, DBQ and idebenone (Ide), were tested. Pilot experiments showed that the effects of DBQ (3 μM) on CI−CIII saturated only after repeated activations over a time period of > 15 min in the presence of the CoQ analogue (data not shown). Therefore, effects of DBQ (3 μM) and Ide (4 μM) on NADH-induced currents were analyzed after repeated NADH activations and over a time period of 17 min. In the presence of DBQ, the NADH-induced currents were increased by ~77%, whereas Ide reduced the currents by ~40% (Figure 3F). The $K_{0.5}$ for NADH in the absence of DBQ was determined to be 17 ± 2 μM (Table 1). In the absence of DBQ, the inhibition with rotenone and antimycin was dose-dependent with calculated IC_{50} values of 0.8 ± 0.3 and 27 ± 3 nM, respectively, and the absolute values of the Hill coefficients were greater than one (Figure 3E and Table 1).

Direct Measurements of CIV Activity. The sensitivity of NADH-induced currents to KCN suggested the involvement of CIV. In addition, the proton pumping activity of CIV was measured directly by performing concentration jumps with reduced cyt *c* (Figure 4A). To prevent spontaneous oxidation, the reduced cyt *c* was applied in the presence of ascorbate (60 μM). Because cyt *c* binds to the intermembrane side of the CIV protein, fresh sensors enriched with intermembrane-side-out (outside-out) membranes were used (Figure 1F and Materials and Methods). Reduced cyt *c* (3 μM) induced negative electrical currents, which was consistent with the movement of positive charges (protons) from the compartment (matrix side) toward the bulk solution [intermembrane side (Figure 4A,B)]. Adding either KCN (1 mM) or NaN_3 (1 mM) to the solutions inhibited the cyt *c*-induced signals (Figure 4B and Figure 2 of the Supporting Information).

Coupled Measurements of CII and CIII. CII is a multimeric enzyme complex associated with the matrix face of the inner mitochondrial membranes. CII catalyzes the conversion

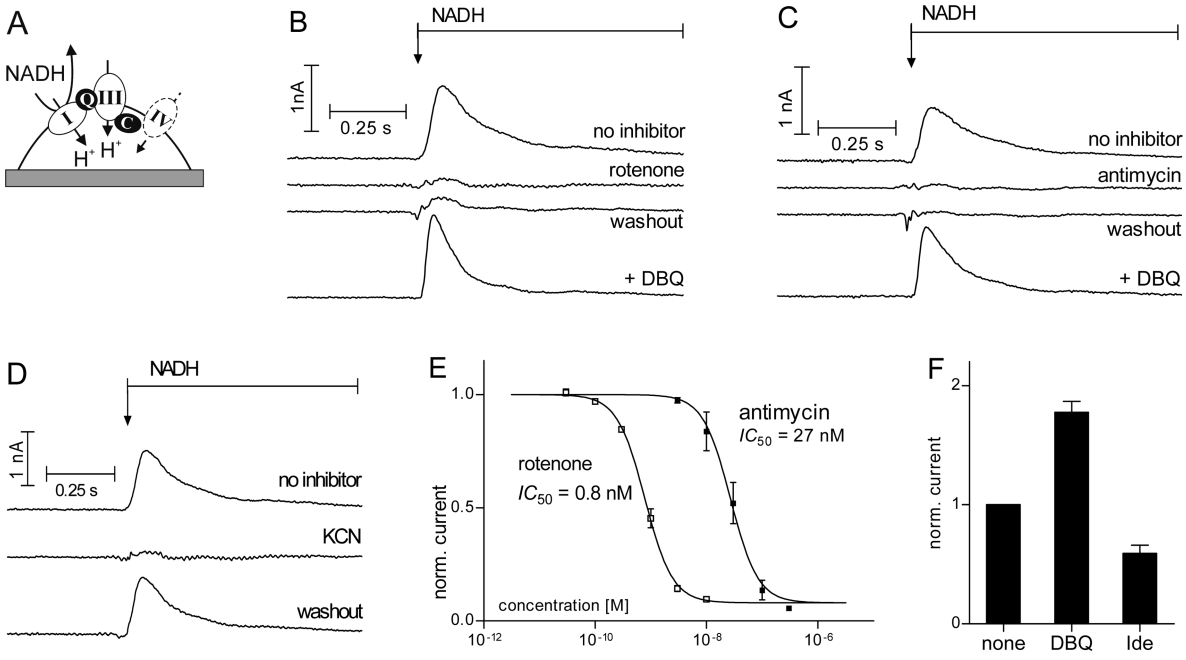

FIGURE 3: CI, CIII, and CIV activities as measured via NADH concentration jumps. (A) NADH-induced transport of protons via CI, CIII, and CIV on SSM sensors. (B−D) NADH (100 μM)-induced currents and inhibition with rotenone (10 nM), antimycin A (300 nM), and KCN (1 mM). Rotenone and antimycin effects were reversed only if decylubiquinone (DBQ, 3 μM) was added to the washout solutions. The top bars indicate the flow of the NADH-containing activating solution. (E) Dependence of NADH (100 μM)-induced currents on increasing rotenone and antimycin concentrations. Currents were normalized relative to the current without the inhibitor. Results are means ± the standard error of the mean for three or four experiments at each concentration. (F) Effects of DBQ (3 μM) and idebenone (Ide, 4 μM) on NADH-induced currents. Currents are relative to the current without the inhibitor or CoQ analog (none).

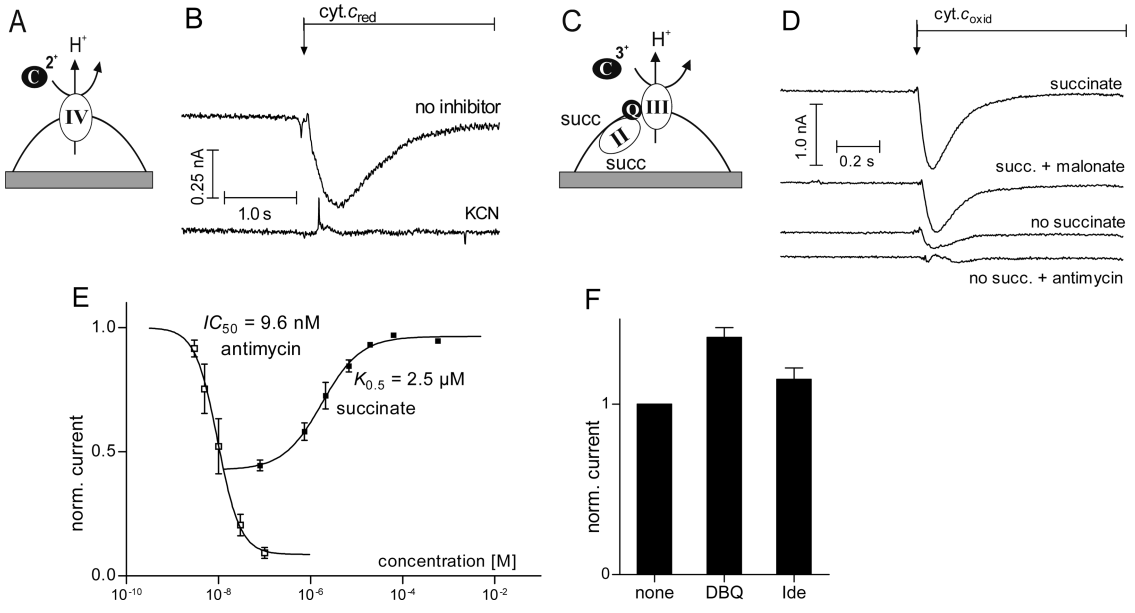

FIGURE 4: CIV and CII−CIII activities as measured via reduced and oxidized cyt *c*, respectively. (A and B) SSM-based principles of the activation of the CIV-dependent proton pumping via reduced cyt *c* (3 μM) and the corresponding KCN (1 mM)-sensitive currents. The measurements were performed in the presence of 60 μM ascorbate. (C and D) SSM-based principles of the activation of CII−CIII-dependent proton pumping through oxidized cyt *c* (3 μM) and the corresponding currents. Succinate (1 mM), malonate (1 mM), and antimycin (30 nM) were applied to the solutions as indicated. The top bars indicate the flow of the cyt *c*-containing, activating solutions. (E) Dependence of cyt c_{oxid}-induced currents on increasing succinate and antimycin concentrations. Antimycin dependence was measured in the presence of 100 μM succinate. Currents were normalized relative to the current at 0.1 mM succinate and to the current without antimycin. Results are means ± the standard error of the mean for four to eight experiments at each concentration. (F) Effects of DBQ (4 μM) and Ide (4 μM) on the cyt c_{oxid}-induced currents. Currents are relative to the current without the inhibitor or CoQ analog (none).

from succinate to fumarate, thereby transferring electrons from succinate to the prosthetic group FAD and generating $FADH_2$ (*24*). The electrons are then transferred from $FADH_2$ via CoQ and CIII to cyt *c*. During this electron translocation process, CIII pumps protons from the matrix to the intermembrane space.

In pilot experiments, the activation of CII and CIII via succinate concentration jumps was tested. However, no succinate-induced currents could be detected (data not shown). Therefore, an alternative approach for activating CII and CIII via oxidized cyt *c* was developed (Figure 4C). Like for CIV (see above), cyt *c* binds to

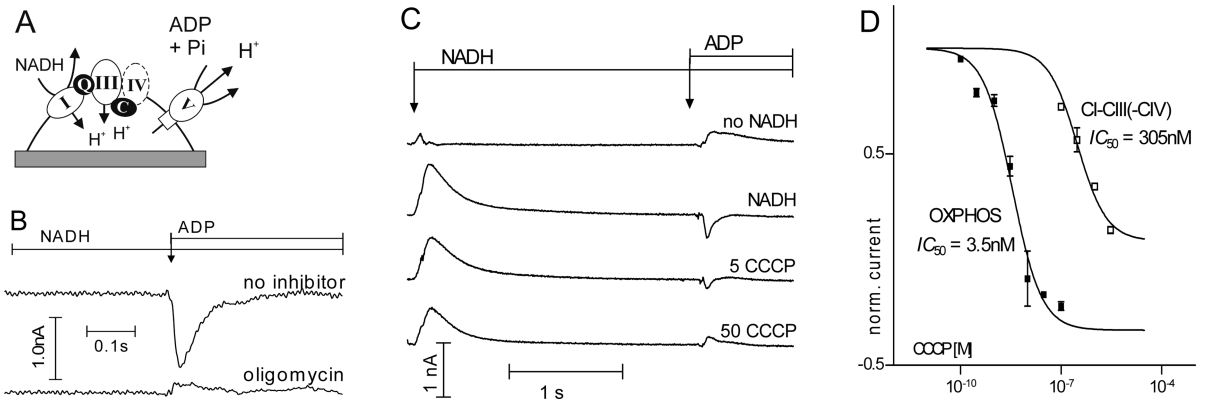

FIGURE 5: F_OF_1-ATP synthase (OXPHOS) activity as measured via ADP concentration jumps and NADH. (A) ADP concentration jumps in the presence of NADH and P_i induce the F_OF_1-ATP synthase on SSM sensors. NADH activates CI, CIII, and CIV, building the outward-directed proton gradient. (B) ADP (300 μM)-induced currents in the presence of NADH (100 μM) and P_i (12 mM), and inhibition with oligomycin (2 μM). (C) Sequential measurements of the NADH (100 μM)-induced and ADP (300 μM)-induced currents, and inhibition with CCCP (nanomolar). (D) Dependence of the NADH- and ADP-induced currents on increasing CCCP concentrations. Currents are relative to the corresponding current without CCCP. Results are means ± the standard error of the mean for four to eight experiments at each concentration. All measurements were performed in the presence of 12 mM P_i and 10 mM $MgCl_2$ on BKA (5 μM)-treated, matrix-side-out enriched sensors [inside-out (Figure 1)]. The top bars indicate the flow of the NADH-containing solutions and the NADH- and ADP-containing solutions.

the intermembrane side of the CIII protein. Therefore, fresh sensors enriched with intermembrane-side-out membranes were preferentially used. In the presence of 1 mM succinate in the nonactivating and activating solutions, the oxidized cyt *c* concentration jumps (3 μM) induced transient negative currents (Figure 4D). The negative sign of the currents was consistent with protons moving away from the sensor toward the bath solution. Addition of the competitive CII inhibitor malonate (1 mM) to the solutions reduced the cyt *c*-induced current (Figure 4D). In the absence of succinate, the cyt *c* concentration jumps induced negative currents, but these currents were significantly smaller than the current in the presence of succinate (Figure 4D). The cyt *c*-induced currents both in the presence and in the absence of succinate were sensitive to the CIII-specific inhibitor antimycin (Figure 4D). The calculated $K_{0.5}$ for succinate was 2.5 ± 0.7 μM (Figure 4E and Table 1). The $IC_{50}^{antimycin}$ of the cyt *c*-induced currents, in the presence of succinate, was 9.6 ± 1.7 nM with an absolute value for the Hill coefficient of ~1.7 (Figure 4E and Table 1). The CoQ analogues DBQ and Ide were analyzed as described for the NADH-induced CI−CIII activities. The application of DBQ (4 μM) and Ide (4 μM) increased the cyt *c*-induced currents by 39 and 15%, respectively (Figure 4F).

F_OF_1-ATPase and Oxidative Phosphorylation (*ATP synthesis*). Conditions for measuring oxidative phosphorylation (OXPHOS, ATP synthesis) were designed in analogy to the physiological conditions in mitochondria. First, activation of CI and CIII (and possibly CIV) via NADH concentration jumps established a proton gradient (Figures 3A and 5A). Subsequently, ATP synthesis was induced by ADP concentration jumps in the presence of inorganic phosphate [P_i (Figure 5A)]. Because NADH and ADP bind to the matrix side of CI and F_OF_1-ATP synthase, frozen sensors enriched with matrix-side-out membranes were preferentially applied (Figure 1E,F and Materials and Methods). Similar to the ATP jumps for measurements of the F_OF_1-ATPase in reverse mode, the ADP concentration jumps can potentially induce ANT transport, thereby interfering with the detection of the ATP synthase activity. Therefore, ANT was inhibited by 5 μM BKA prior to the F_OF_1-ATP synthase measurements. Consistent with the movement of protons away from the sensor electrode, the ADP concentration jumps (300 μM) induced negative currents that were inhibited by the F_OF_1-specific inhibitor oligomycin [2 μM (Figure 5B)]. To study the influence of a proton gradient on the F_OF_1-ATP synthase, both NADH-induced and ADP-induced currents were monitored simultaneously during the same electrical recording (Figure 5C). ADP concentration jumps (300 μM) in the absence of a proton gradient (measurements without NADH) induced small but distinct positive currents (Figure 5C). Sequential application of NADH (100 μM) and ADP (300 μM) resulted in positive and negative currents, respectively. The sign of the currents was consistent with the movement of protons toward (NADH) and away from (ADP) the electrode. At 5 nM, the proton uncoupling agent carbonyl cyanide 3-chlorophenylhydrazone (CCCP) dramatically decreased the ADP-induced currents, while the NADH-induced currents were not affected. Increasing the CCCP concentration to 50 nM abolished the ADP-dependent currents, whereas the NADH-dependent signals were affected to an only minor extent (Figure 5C). The calculated IC_{50}^{CCCP} of 3.5 nM for the ADP-induced current was 100 times lower than the IC_{50}^{CCCP} of 305 nM determined for the NADH-induced signal (Figure 5D and Table 1).

DISCUSSION

The interplay among the respiratory chain proteins and transporters of inner mitochondrial membranes is essential for the regulation of many physiological processes such as oxidative stress, Ca^{2+} homeostasis, and thermogenesis (*25*, *26*). Therefore, direct functional analysis of mitochondrial transport proteins in their native environment is important for the understanding of fundamental functions of the eukaryotic cell. This work describes a new SSM-based approach for electrophysiological, mechanistic, and pharmacological studies of the respiratory chain complexes and ANT.

SSM-Based Currents and Activities of the Electron Transport Chain Proteins. According to the principles of the SSM-based electrophysiology, the protein-dependent currents correspond to the charging of a capacitor. As expected for capacitor charging, all reported substrate-induced currents were transient with decay times of several hundred milliseconds, which is well within the range of currents reported in other SSM-based studies (*12*, *13*, *16*). Apart from the translocation of charged

substrates and cosubstrates (vectorial transport), the SSM technology can also detect other electrogenic events associated with the activity of transport proteins, such as binding of a charged substrate to the protein or a movement of protein innate charges upon the binding of an electroneutral substrate (*27*−*29*). Accordingly, the SSM technology can detect any charge movements within the electric field of the membrane. In the case of mitochondrial respiratory chain complexes CI, CIII, and CIV, vectorial transport of protons, as well as the movement of electrons and of accompanying "chemical" protons, may in principle be detected. The positive sign of the NADH-induced, CI−CIII-dependent electrical currents was consistent with the flow of protons from the bulk solution (matrix side) to the fluid-filled compartments on the sensor electrode (*14*, *16*, *17*). In contrast, transport of electrons from NADH on the matrix side toward cyt *c* at the intermembrane side would be expected to induce negative currents (*23*). Therefore, the sign of the CI−CIII-dependent currents shows that proton transport accounts for the major portion of the NADH-induced electric signal. Both the chemical protons and the excess of the vectorial protons apparently compensate for the electron movements. Alternatively, electron backflow to the matrix side via cyt *c* and CIV may neutralize the initial electron motion. Similarly, the negative sign of the cyt *c*-induced currents in the CII−CIII assay was consistent with the transport of protons away from the fluid-filled compartment toward the bulk solution, whereas electron transport was expected to induce currents with a positive sign. Thus, even though the sum of all electrogenic steps is measured upon NADH or cyt *c* application in these assays, the polarity (sign) of the signals suggests that the electric activities represent mainly the vectorial proton transport catalyzed by CI and CIII. The situation is somewhat different in the case of the direct measurements of the CIV activity. Here, the negative sign of the currents correlates with the vectorial proton transport from the fluid-filled compartments [matrix side (Figure 4A)] as well as with the transfer of electrons from cyt *c* to the O_2 reduction site of the enzyme [i.e., from bulk solutions to the compartment (*30*, *31*)]. Therefore, the polarity of the signals in the described CIV measurements does not allow us to judge whether the vectorial proton transport represents the major part of the electric activity. Nevertheless, compensation of the electron movement by chemical protons is highly probable.

Electrical and Pharmacological Characteristics of the Native ANT Activity. The major function of ANT is the exchange of one ATP^{4-} from the matrix with one ADP^{3-} from the intermembrane space. This heteroexchange brings about a surplus of negative charge with each transported ATP^{4-} molecule. Consistent with the movement of ATP-derived negative charge into or out of the fluid-filled compartments on the sensor (Figure 1A), ATP and ADP concentration jumps in the presence of outward-directed ADP and ATP counter gradients induced negative and positive electrical currents, respectively. Previous experiments with the reconstituted ANT protein have shown that beside the ATP−ADP heteroexchange, ANT can also transport only ATP or ADP (*13*, *32*). Under such conditions, the translocation of one ATP^{4-} molecule is coupled to the movement of negative charge, while the translocation of one ADP^{3-} results in positive charge movements due to the positive countercharges (~3.3) of the nucleotide binding pockets (*13*, *32*). Accordingly, ADP and ATP jumps induced currents with opposite signs in the absence of outward-directed nucleotide gradients. Under these conditions, ANT transports one nucleotide molecule and then either stops or switches over to an ATP−ATP or ADP−ADP homoexchange mode that does not generate electric currents (*32*). In contrast, in the presence of nucleotide counter gradients, nucleotide jumps trigger a repetitive electrogenic ATP−ADP heteroexchange. Therefore, the ATP- and ADP-induced currents in the absence of nucleotide counter gradients were always smaller and decaying faster than corresponding currents under heteroexchange conditions.

The sensitivity of the ADP- and ATP-induced signals to the ANT inhibitors CAT and BKA demonstrates the specificity of the signals. The calculated $K_{0.5}^{ADP}$ (42 μM) and $K_{0.5}^{ATP}$ (8 μM) measured in the presence of the respective gradients were similar to the previously published $K_{0.5}$ values varying from 1−30 μM for ADP to 1−140 μM for ATP (*2*). The large $K_{0.5}$ variations were explained by different experimental conditions as well as different ANT sources. For the SSM measurements using ANT reconstituted in liposomes, the $K_{0.5}^{ATP}$ was estimated to be 20 μM (*13*), which fits well with the $K_{0.5}^{ATP}$ of 8 μM for the native ANT in our measurements. Many studies suggest that the functional unit of ANT is a homodimer transporting two molecules of adenylates at a time in opposite directions (*2*, *33*−*35*). Alternatively, experiments with yeast ANT suggested that the protein could also function as a monomer (*36*, *37*). Similarly, the cooperativity of adenylate binding sites is still an open question (*2*, *33*). In our experiments, ADP and ATP dependencies fit well with single-binding site kinetics (Hill coefficient of ~1), supporting the model in which the binding of the nucleotide to the functional ANT unit is not cooperative. Moreover, the $K_{0.5}^{ATP}$ was the same in the presence or absence of an outward-directed ADP gradient, further supporting the idea that binding of a nucleotide at one site does not influence the binding of the second nucleotide.

F_OF_1-ATPase: Reverse and Forward Mode, Uncoupling, and Membrane Potential. The major role of the F_OF_1-ATPase is to synthesize ATP at the expense of the membrane potential built up by the proton-pumping respiratory chain complexes. In this so-called "forward mode", the F_OF_1-ATPase is also defined as an ATP synthase. Besides, F_OF_1-ATPase can also function as an ATPase, catalyzing ATP hydrolysis and pumping protons into the matrix ["reverse mode" (*21*)]. In SSM experiments, the positive sign of the ATP-induced currents corresponds to the pumping of protons across the membranes toward the sensor electrode via the reverse mode activity of the F_OF_1-ATPase. The specificity of the positive ATP-induced currents was demonstrated by their sensitivity to the F_OF_1-ATPase inhibitors oligomycin, DCCD, and azide (*21*, *22*, *38*). The calculated IC_{50} for azide was in good agreement with previous studies (*39*). The time- and concentration-dependent inhibition and the irreversibility of DCCD reflect the fact that DCCD forms stable covalent bonds with the F_OF_1-ATPase protein (*22*, *40*). The F_OF_1-ATPase proton pumping activity depended on the ATP concentration to the first power (Hill coefficient of ~1) with an apparent $K_{0.5}$ (45 ± 5 μM) well within the range of published values from 38 to 140 μM (*12*, *39*, *41*).

The SSM-based ATP synthase assay consists of an ADP concentration jump in the presence of Mg^{2+}, phosphate (P_i), and a proton gradient built upon NADH application. Under these conditions, the negative sign of the ADP-induced currents represents the proton flux from the fluid-filled compartments across the adsorbed membranes to the bath solution and corresponds to the F_OF_1-ATP synthase activity as demonstrated by the inhibition with the F_OF_1-ATPase-specific inhibitor oligomycin. In all ATP synthase experiments, the ANT "background" activity had

to be blocked with BKA and a high Mg^{2+} concentration; otherwise, the negative ATP synthase-specific currents were masked by the positive currents of the ADP-transporting ANT (data not shown). Interestingly, ADP jumps induced small positive currents even after the ANT blockage when measured in the absence of a proton gradient (without NADH). Because of the presence of BKA and a high Mg^{2+} concentration inhibiting ANT, it is improbable that these currents originate from a residual ANT activity. These signals may rather represent activities of other ADP- and Mg^{2+}-dependent transport proteins (*25*, *42*, *43*).

The inhibition of the F_OF_1-ATPase-specific ADP-induced currents by the protonophore and uncoupler CCCP is consistent with the fact that proton gradients are essential for ATP synthesis (*22*, *44*). Interestingly, the ATP synthase was ~100 times more sensitive to CCCP (IC_{50} = 3.5 nM) than the NADH-induced currents representing the coupled activities of the CI, CIII, and CIV proton pumps. This differential CCCP effect is based on the transport processes underlying the NADH-induced currents and on the transport mechanism of the ATP synthase. With NADH concentration jumps, proton pumps CI and CIII generate currents until a maximum membrane potential is reached. Therefore, the CCCP does not inhibit the NADH-dependent currents by a reduction of the proton pump activities but rather provides a short circuit for protons, thereby reducing the maximum possible membrane potential. Accordingly, the CCCP concentration necessary for full inhibition of the NADH-induced currents is ~1 mM, a concentration that is usually applied to completely dissipate mitochondrial membrane potential (*45*, *46*). On the other hand, membrane potential is the major driving force for ATP synthesis. Therefore, dissipation of the membrane potential by CCCP directly reduces the activity of the F_OF_1-ATP synthase. The dependence of the F_OF_1-ATP synthase on the proton motive force is not linear, but a minimal threshold membrane potential is needed for the activation of the F_OF_1-ATP synthase (*22*, *47*). Therefore, CCCP concentrations (~10 nM) at which the synthase-specific currents are just about fully inhibited reduce the membrane potential to such threshold values. These results demonstrate that the SSM-based approach allows the identification of drugs, which affect the mitochondrial function by partial depolarization.

Complexes CI, CIII, and CIV and Their Functional Coupling. CI is the first complex of the respiratory chain catalyzing the oxidation of NADH, reducing CoQ, and pumping protons from the matrix into the intermembrane space (*23*). On one hand, the NADH-induced currents showed an apparent $K_{0.5}$ for NADH of 17 μM, which is in good agreement with the $K_{0.5}^{NADH}$ values of 10−40 μM determined for CI activity (*48*, *49*). Additionally, the apparent $IC_{50}^{rotenone}$ of 0.8 nM is similar to the CI-specific values of 4−20 nM described in literature (*48*−*51*). On the other hand, the data on the number of rotenone binding sites are controversial. While Degli Esposti (*50*) suggests one, Mehta et al. (*52*) described two rotenone binding sites on the CI protein. With SSM-based electrophysiology, the absolute value of the Hill coefficient for rotenone was 1.7 ± 0.3, suggesting that multiple binding sites with positive cooperativity might exist. The effects of a high rotenone concentration (2 μM) were irreversible, whereas after the application of a low concentration of rotenone (10 nM), the NADH-dependent signals could be re-established when the CoQ analogue DBQ was added to the solutions. This is in contrast to studies showing that rotenone does not compete with CoQ analogues (*50*). Further studies are necessary to elucidate the impact of DBQ on rotenone binding and CI function.

In the respiratory chain reaction, CoQ accepts the electrons from NADH and transfers them to CIII. CIII oxidizes CoQ, which is then available again for CI (*26*, *53*). Thus, CoQ and the functional CIII are both necessary for repetitive activations of CI in the SSM experiments. The NADH-induced currents were routinely observed in the absence of CoQ analogues and could be fully inhibited by the CIII inhibitor antimycin, demonstrating that the endogenous CoQ pool and the CIII protein in the mitochondrial membranes were sufficient and essential for the maintenance of CI activity. Furthermore, the antimycin-inhibited, NADH-dependent signals could be restored when the oxidized CoQ analogue DBQ was supplied to the solutions, thereby replacing the endogenous CoQ. Therefore, it is possible to measure CI separately with solutions containing antimycin to suppress reoxidation of endogenous CoQ and DBQ acting as an artificial electron acceptor for the NADH dehydrogenase. The apparent IC_{50} value for antimycin of 27 nM and the steep slope of the curve (absolute value for the Hill coefficient of > 1) were in agreement with previously published results (*51*). Functional CI−CIII coupling was further characterized by two different CoQ analogues, DBQ and an antioxidant drug idebenone (Ide). In the absence of antimycin, DBQ stimulated NADH-induced currents, whereas Ide reduced them. This differential behavior is in line with DBQ being a good substrate of CI, whereas Ide is a poor substrate and can inhibit CI activity (*54*, *55*).

The proton pumping activity of CIII is coupled to the transfer of electrons to cyt *c*. The resulting reduced cyt *c* is then reoxidized by CIV. Therefore, if the oxidized cyt *c* is limited, CIV is needed for cyt *c* recycling and CIII activity. The fact that the NADH-induced CI−CIII activity was routinely observed without an additional supply of oxidized cyt *c* demonstrates that the inner mitochondrial membranes contain sufficient amounts of endogenous cyt *c* and suggests that CIV may participate in the NADH-induced electric response by recycling of the cyt *c*. Different CIV inhibitors were applied to study the involvement of CIV in the NADH-induced response. Cyanide (KCN) is a standard inhibitor of CIV (*56*, *57*), and it can also bind to oxidized (ferric) but not to reduced (ferrous) cyt *c* (*58*). Therefore, the sensitivity of NADH-induced, CI−CIII-dependent signals to KCN can be interpreted either by the inhibition of CIV and cyt *c* recycling or by the direct binding of KCN to oxidized cyt *c*. Interestingly, sodium azide [NaN_3, another CIV inhibitor (*31*, *57*)] did not influence the CI−CIII-dependent currents, suggesting that the KCN inhibition may rather reflect KCN binding to the oxidized cyt *c* (Figure 1 of the Supporting Information). On the other hand, direct activation of CIV via reduced cyt *c* jumps and the inhibition of the corresponding currents with KCN and NaN_3 clearly demonstrate that functional CIV is present in the membranes (Figure 4B and Figure 2 of the Supporting Information). At the current state of the study, we cannot definitively decide whether the KCN effects are due to inhibition of CIV or reduction of the oxidized cyt *c* pool, and whether the NADH-induced currents correspond to the coupled CI−CIII or CI−CIII−CIV activities. However, "isolated" CIV-independent CI−CIII activity may be interesting in the context of the supramolecular organization of the respiratory chain and its physiological impact on the mitochondrial function (*4*, *59*, *60*).

Complexes CII and CIII. CII transfers electrons from succinate to CoQ, thereby triggering CIII-dependent proton pumping (*24*, *61*). Because CII itself neither pumps protons nor translocates electrons across the mitochondrial membranes, the electrical characterization of CII was based on measuring the

CIII activity. In pilot experiments, succinate concentration jumps did not induce any significant CII−CIII-dependent currents (data not shown). This was inconsistent with the ability to activate the CI−CIII reactions via NADH jumps. One possible explanation may be that the succinate-triggered reactions are desynchronized, and therefore, CIII-dependent H^+ pumping cannot be observed as an immediate succinate-induced electric current. Such relative desynchronization of the CII−CIII activities in comparison to the CI−CIII reactions may be due to the use of different CoQ pools by the CII and CI complexes (*53*, *59*). To circumvent this problem, we measured the CII−CIII activity via oxidized cyt *c* jumps in the presence of succinate. Similar to the CI−CIII (CIV) assay, the endogenous CoQ pool was sufficient for the CII−CIII reaction. The calculated $K_{0.5}^{\text{succinate}}$ of 2.5 μM was lower than the value of 40 μM reported in the literature (*24*, *61*). On the other hand, the calculated $IC_{50}^{\text{antimycin}}$ of 9.6 nM and the Hill coefficient were similar to the values determined by the NADH-induced CI−CIII assay and well within the range of previously published results, demonstrating the specificity of the CII−CIII assay [Table 1 (*51*)]. The specificity was further demonstrated by the inhibition with the CII inhibitor malonate. Finally, the detected stimulating effects of Ide and DBQ on the CII−CIII activity correlate with results published previously (*54*). At the current state of the project, we have no convincing explanation for the origin of the antimycin-sensitive but succinate-independent, cyt *c*-induced currents (Figure 4D). It is possible these currents may reflect some transient charge translocations in the CIII reaction centers.

CONCLUSIONS

Direct functional investigation of the respiratory chain and transporters in their native environment is important for the understanding of many essential physiological functions. The experiments described in this work demonstrate that the SSM technique is a powerful method for the pharmacological investigation of electrogenic transport processes in native inner mitochondrial membranes. Monitoring the activity of transport proteins by direct detection of charge movements allows new insights into the mechanistic work of mitochondrial transport proteins and can help in further understanding the complex interplay of respiratory chain proteins and of the functional roles of such interplay in respiration and oxidative phosphorylation. Furthermore, the F_OF_1-ATP synthase assay provides a highly sensitive tool for the detection of uncoupling agents and pharmacologically relevant CoQ analogues. Thus, the technology proves to be a versatile platform for general as well as detailed mechanistic and pharmacological studies of proteins and electrogenic processes of inner mitochondrial membranes.

ACKNOWLEDGMENT

We are grateful to Robin Krause for critical reading of the manuscript.

SUPPORTING INFORMATION AVAILABLE

Effects of NaN_3 on NADH-induced currents and on CIV-specific currents. This material is available free of charge via the Internet at http://pubs.acs.org.

REFERENCES

1. Mitchell, P. (1961) Coupling of phosphorylation to electron and hydrogen transfer by a chemi-osmotic type of mechanism. *Nature 191*, 144–148.
2. Klingenberg, M. (2008) The ADP and ATP transport in mitochondria and its carrier. *Biochim. Biophys. Acta 1778*, 1978–2021.
3. Vignais, P. V., Douce, R., Lauquin, G. J., and Vignais, P. M. (1976) Binding of radioactively labeled carboxyatractyloside, atractyloside and bongkrekic acid to the ADP translocator of potato mitochondria. *Biochim. Biophys. Acta 440*, 688–696.
4. Acin-Perez, R., Fernandez-Silva, P., Peleato, M. L., Perez-Martos, A., and Enriquez, J. A. (2008) Respiratory active mitochondrial supercomplexes. *Mol. Cell 32*, 529–539.
5. Boekema, E. J., and Braun, H. P. (2007) Supramolecular structure of the mitochondrial oxidative phosphorylation system. *J. Biol. Chem. 282*, 1–4.
6. Kinnally, K. W., Campo, M. L., and Tedeschi, H. (1989) Mitochondrial channel activity studied by patch-clamping mitoplasts. *J. Bioenerg. Biomembr. 21*, 497–506.
7. Kirichok, Y., Krapivinsky, G., and Clapham, D. E. (2004) The mitochondrial calcium uniporter is a highly selective ion channel. *Nature 427*, 360–364.
8. Szabo, I., Bock, J., Jekle, A., Soddemann, M., Adams, C., Lang, F., Zoratti, M., and Gulbins, E. (2005) A novel potassium channel in lymphocyte mitochondria. *J. Biol. Chem. 280*, 12790–12798.
9. Thieffry, M., Neyton, J., Pelleschi, M., Fevre, F., and Henry, J. P. (1992) Properties of the mitochondrial peptide-sensitive cationic channel studied in planar bilayers and patches of giant liposomes. *Biophys. J. 63*, 333–339.
10. Herick, K., Kramer, R., and Luhring, H. (1997) Patch clamp investigation into the phosphate carrier from *Saccharomyces cerevisiae* mitochondria. *Biochim. Biophys. Acta 1321*, 207–220.
11. Huang, S. G., and Klingenberg, M. (1996) Chloride channel properties of the uncoupling protein from brown adipose tissue mitochondria: A patch-clamp study. *Biochemistry 35*, 16806–16814.
12. Burzik, C., Kaim, G., Dimroth, P., Bamberg, E., and Fendler, K. (2003) Charge displacements during ATP-hydrolysis and synthesis of the Na^+-transporting FoF1-ATPase of *Ilyobacter tartaricus*. *Biophys. J. 85*, 2044–2054.
13. Gropp, T., Brustovetsky, N., Klingenberg, M., Muller, V., Fendler, K., and Bamberg, E. (1999) Kinetics of electrogenic transport by the ADP/ATP carrier. *Biophys. J. 77*, 714–726.
14. Obrdlik, P., Diekert, K., Watzke, N., Keipert, C., Pehl, U., Brosch, C., Boehm, N., Bick, I., Ruitenberg, M., Volknandt, W., and Kelety, B. (2010) Electrophysiological characterization of ATPases in native synaptic vesicles and synaptic plasma membranes. *Biochem. J. 427*, 151–159.
15. Pintschovius, J., and Fendler, K. (1999) Charge translocation by the Na^+/K^+-ATPase investigated on solid supported membranes: Rapid solution exchange with a new technique. *Biophys. J. 76*, 814–826.
16. Kelety, B., Diekert, K., Tobien, J., Watzke, N., Dorner, W., Obrdlik, P., and Fendler, K. (2006) Transporter assays using solid supported membranes: A novel screening platform for drug discovery. *Assay Drug Dev. Technol. 4*, 575–582.
17. Schulz, P., Garcia-Celma, J. J., and Fendler, K. (2008) SSM-based electrophysiology. *Methods 46*, 97–103.
18. Blair, P. V. (1967) The large-scale preparation and properties of heart mitochondria from slaughterhouse material. *Methods Enzymol. 10*, 78–81.
19. Hovius, R., Lambrechts, H., Nicolay, K., and de Kruijff, B. (1990) Improved methods to isolate and subfractionate rat liver mitochondria. Lipid composition of the inner and outer membrane. *Biochim. Biophys. Acta 1021*, 217–226.
20. Boyer, P. D. (1975) A model for conformational coupling of membrane potential and proton translocation to ATP synthesis and to active transport. *FEBS Lett. 58*, 1–6.
21. Vinogradov, A. D. (2000) Steady-state and pre-steady-state kinetics of the mitochondrial F_1F_o ATPase: Is ATP synthase a reversible molecular machine? *J. Exp. Biol. 203*, 41–49.
22. von Ballmoos, C., Cook, G. M., and Dimroth, P. (2008) Unique rotary ATP synthase and its biological diversity. *Annu. Rev. Biophys. 37*, 43–64.
23. Kerscher, S., Drose, S., Zickermann, V., and Brandt, U. (2008) The three families of respiratory NADH dehydrogenases. *Results Probl. Cell Differ. 45*, 185–222.
24. Ackrell, B. A. (2000) Progress in understanding structure-function relationships in respiratory chain complex II. *FEBS Lett. 466*, 1–5.
25. Palmieri, F. (2008) Diseases caused by defects of mitochondrial carriers: A review. *Biochim. Biophys. Acta 1777*, 564–578.
26. Szewczyk, A., and Wojtczak, L. (2002) Mitochondria as a pharmacological target. *Pharmacol. Rev. 54*, 101–127.
27. Meyer-Lipp, K., Ganea, C., Pourcher, T., Leblanc, G., and Fendler, K. (2004) Sugar binding induced charge translocation in the melibiose permease from *Escherichia coli*. *Biochemistry 43*, 12606–12613.

28. Tadini-Buoninsegni, F., Bartolommei, G., Moncelli, M. R., and Fendler, K. (2008) Charge transfer in P-type ATPases investigated on planar membranes. *Arch. Biochem. Biophys. 476*, 75–86.
29. Zhou, A., Wozniak, A., Meyer-Lipp, K., Nietschke, M., Jung, H., and Fendler, K. (2004) Charge translocation during cosubstrate binding in the Na^+/proline transporter of *E. coli*. *J. Mol. Biol. 343*, 931–942.
30. Brzezinski, P. (1996) Internal electron-transfer reactions in cytochrome c oxidase. *Biochemistry 35*, 5611–5615.
31. Yoshikawa, S., Shinzawa-Itoh, K., Nakashima, R., Yaono, R., Yamashita, E., Inoue, N., Yao, M., Fei, M. J., Libeu, C. P., Mizushima, T., Yamaguchi, H., Tomizaki, T., and Tsukihara, T. (1998) Redox-coupled crystal structural changes in bovine heart cytochrome c oxidase. *Science 280*, 1723–1729.
32. Brustovetsky, N., Becker, A., Klingenberg, M., and Bamberg, E. (1996) Electrical currents associated with nucleotide transport by the reconstituted mitochondrial ADP/ATP carrier. *Proc. Natl. Acad. Sci. U.S.A. 93*, 664–668.
33. Metelkin, E., Goryanin, I., and Demin, O. (2006) Mathematical modeling of mitochondrial adenine nucleotide translocase. *Biophys. J. 90*, 423–432.
34. Nury, H., Dahout-Gonzalez, C., Trezeguet, V., Lauquin, G., Brandolin, G., and Pebay-Peyroula, E. (2005) Structural basis for lipid-mediated interactions between mitochondrial ADP/ATP carrier monomers. *FEBS Lett. 579*, 6031–6036.
35. Pebay-Peyroula, E., Dahout-Gonzalez, C., Kahn, R., Trezeguet, V., Lauquin, G. J., and Brandolin, G. (2003) Structure of mitochondrial ADP/ATP carrier in complex with carboxyatractyloside. *Nature 426*, 39–44.
36. Bamber, L., Harding, M., Monne, M., Slotboom, D. J., and Kunji, E. R. (2007) The yeast mitochondrial ADP/ATP carrier functions as a monomer in mitochondrial membranes. *Proc. Natl. Acad. Sci. U.S.A. 104*, 10830–10834.
37. Bamber, L., Slotboom, D. J., and Kunji, E. R. (2007) Yeast mitochondrial ADP/ATP carriers are monomeric in detergents as demonstrated by differential affinity purification. *J. Mol. Biol. 371*, 388–395.
38. Vinogradov, A. D. (1999) Mitochondrial ATP synthase: Fifteen years later. *Biochemistry* (*Moscow, Russ. Fed.*) *64*, 1219–1229.
39. Vasilyeva, E. A., Minkov, I. B., Fitin, A. F., and Vinogradov, A. D. (1982) Kinetic mechanism of mitochondrial adenosine triphosphatase. Inhibition by azide and activation by sulphite. *Biochem. J. 202*, 15–23.
40. Kluge, C., and Dimroth, P. (1993) Kinetics of inactivation of the F1Fo ATPase of *Propionigenium modestum* by dicyclohexylcarbodiimide in relationship to H^+ and Na^+ concentration: Probing the binding site for the coupling ions. *Biochemistry 32*, 10378–10386.
41. Reynafarje, B. D., and Pedersen, P. L. (1996) ATP synthase. Conditions under which all catalytic sites of the F1 moiety are kinetically equivalent in hydrolyzing ATP. *J. Biol. Chem. 271*, 32546–32550.
42. Fiermonte, G., De Leonardis, F., Todisco, S., Palmieri, L., Lasorsa, F. M., and Palmieri, F. (2004) Identification of the mitochondrial ATP-Mg/Pi transporter. Bacterial expression, reconstitution, functional characterization, and tissue distribution. *J. Biol. Chem. 279*, 30722–30730.
43. Palmieri, F. (2004) The mitochondrial transporter family (SLC25): Physiological and pathological implications. *Pfluegers Arch. 447*, 689–709.
44. Knox, B. E., and Tsong, T. Y. (1984) Voltage-driven ATP synthesis by beef heart mitochondrial F0F1-ATPase. *J. Biol. Chem. 259*, 4757–4763.
45. Geissler, A., Krimmer, T., Bomer, U., Guiard, B., Rassow, J., and Pfanner, N. (2000) Membrane potential-driven protein import into mitochondria. The sorting sequence of cytochrome b_2 modulates the $\Delta\psi$-dependence of translocation of the matrix-targeting sequence. *Mol. Biol. Cell 11*, 3977–3991.
46. Scaduto, R. C., Jr., and Grotyohann, L. W. (1999) Measurement of mitochondrial membrane potential using fluorescent rhodamine derivatives. *Biophys. J. 76*, 469–477.
47. Thayer, W. S., and Hinkle, P. C. (1975) Kinetics of adenosine triphosphate synthesis in bovine heart submitochondrial particles. *J. Biol. Chem. 250*, 5336.
48. Higgins, D. S., Jr., and Greenamyre, J. T. (1996) [^{3}H]Dihydrorotenone binding to NADH: Ubiquinone reductase (complex I) of the electron transport chain: An autoradiographic study. *J. Neurosci. 16*, 3807–3816.
49. Janssen, A. J., Trijbels, F. J., Sengers, R. C., Smeitink, J. A., van den Heuvel, L. P., Wintjes, L. T., Stoltenborg-Hogenkamp, B. J., and Rodenburg, R. J. (2007) Spectrophotometric assay for complex I of the respiratory chain in tissue samples and cultured fibroblasts. *Clin. Chem. 53*, 729–734.
50. Degli Esposti, M. (1998) Inhibitors of NADH-ubiquinone reductase: An overview. *Biochim. Biophys. Acta 1364*, 222–235.
51. Nadanaciva, S., Bernal, A., Aggeler, R., Capaldi, R., and Will, Y. (2007) Target identification of drug induced mitochondrial toxicity using immunocapture based OXPHOS activity assays. *Toxicol. in Vitro 21*, 902–911.
52. Mehta, R., Chan, K., Lee, O., Tafazoli, S., and O'Brien, P. J. (2008) Drug-Associated Mitochondrial Toxicity. In Drug-induced Mitochondrial Dysfunction (Dykens, J. A., and Will, Y., Eds.) John Wiley & Sons, New York.
53. Lenaz, G., and Genova, M. L. (2009) Mobility and function of coenzyme Q (ubiquinone) in the mitochondrial respiratory chain. *Biochim. Biophys. Acta 1787*, 563–573.
54. Briere, J. J., Schlemmer, D., Chretien, D., and Rustin, P. (2004) Quinone analogues regulate mitochondrial substrate competitive oxidation. *Biochem. Biophys. Res. Commun. 316*, 1138–1142.
55. Esposti, M. D., Ngo, A., Ghelli, A., Benelli, B., Carelli, V., McLennan, H., and Linnane, A. W. (1996) The interaction of Q analogs, particularly hydroxydecyl benzoquinone (idebenone), with the respiratory complexes of heart mitochondria. *Arch. Biochem. Biophys. 330*, 395–400.
56. Kannt, A., Pfitzner, U., Ruitenberg, M., Hellwig, P., Ludwig, B., Mantele, W., Fendler, K., and Michel, H. (1999) Mutation of Arg-54 strongly influences heme composition and rate and directionality of electron transfer in *Paracoccus denitrificans* cytochrome c oxidase. *J. Biol. Chem. 274*, 37974–37981.
57. Mitchell, R., and Rich, P. R. (1994) Proton uptake by cytochrome c oxidase on reduction and on ligand binding. *Biochim. Biophys. Acta 1186*, 19–26.
58. Schejter, A., Ryan, M. D., Blizzard, E. R., Zhang, C., Margoliash, E., and Feinberg, B. A. (2006) The redox couple of the cytochrome c cyanide complex: The contribution of heme iron ligation to the structural stability, chemical reactivity, and physiological behavior of horse cytochrome c. *Protein Sci. 15*, 234–241.
59. Lenaz, G., and Genova, M. L. (2007) Kinetics of integrated electron transfer in the mitochondrial respiratory chain: Random collisions vs. solid state electron channeling. *Am. J. Physiol. 292*, C1221–C1239.
60. Dudkina, N. V., Eubel, H., Keegstra, W., Boekema, E. J., and Braun, H. P. (2005) Structure of a mitochondrial supercomplex formed by respiratory-chain complexes I and III. *Proc. Natl. Acad. Sci. U.S.A. 102*, 3225–3229.
61. Kolker, S., Schwab, M., Horster, F., Sauer, S., Hinz, A., Wolf, N. I., Mayatepek, E., Hoffmann, G. F., Smeitink, J. A., and Okun, J. G. (2003) Methylmalonic acid, a biochemical hallmark of methylmalonic acidurias but no inhibitor of mitochondrial respiratory chain. *J. Biol. Chem. 278*, 47388–47393.